Surface-Enhanced Raman Scattering in Noble-Metal Nanoparticles: A Microscopic Approach

Vitaliy N. Pustovit, Tigran V. Shahbazyan
Department of Physics and Computational Center for Molecular Structure and Interactions
Jackson State University, Jackson, MS 39217, USA

Abstract

We present a microscopic model for surface-enhanced Raman scattering (SERS) from molecules adsorbed on small noble-metal nanoparticles. We demonstrate that, in nanometer-sized particles, SERS is determined by a competition between two distinct quantum-size effects: Landau damping of surface plasmon resonance and reduced screening near nanoparticle surface. The first mechanism comes from the discreteness of energy spectrum in a nanoparticle and leads to a general decrease in SERS. The second mechanism originates from the different effect of confining potential on *sp*-band and *d*-band electron states and leads to relative increase in SERS. We calculate numerically the spatial distribution of local field near the surface and the enhancement factor for different nanoparticles sizes.

1 Introduction

Surface-enhanced Raman scattering (SERS) has been one of the highlights of optical spectroscopy in metal nanostructures during past 25 years [1]. A renewed interest in SERS stems from the discovery of extremely strong single-molecule SERS in silver nanoparticle aggregates [2,3], and from numerous nanoparticle-based applications such as, e.g., biosensors [4] that rely on sensitivity of SERS to small concentrations of target molecules. The main mechanism of SERS has long been known as electromagnetic (EM) enhancement [1,5–7] of dipole moment of a molecule by strong local field of surface plasmon (SP) resonance in a nanoparticle. EM mechanism is especially effective when a cluster of nanoparticles is concentrated in a small spatial region ("hot spot") [8–11]. A combined effect of SP local fields from different particles acting on a molecule trapped in a gap can result in a giant (up to 10^{14}) enhancement of the Raman scattering crossection [12–15]. Other mechanisms contributing to SERS can involve electron tunneling between a molecule and a nanoparticle [16].

The conventional description of EM enhancement is based on classical Mie scattering theory [6, 7]. The dipole moment of a molecule at distance $\mathbf{r}_0$ form a particle center is enhanced by a factor $\sim \alpha_p(\omega)/r_0^3$, where $\alpha_p = R^3\,\frac{\epsilon-1}{\epsilon+2}$ is the particle polarizability, R is its radius, and $\epsilon(\omega)$ is metal dielectric function. The far-field of molecular dipole, radiating at Stokes-shifted frequency ω_s, is, in turn, comprised of direct and Mie-scattered fields. The latter contributes another factor $\sim \alpha_p(\omega_s)/r_0^3$, so that the Raman crossection is proportional to $|\alpha_p|^4/r_0^{12}$. At frequencies close to the SP pole in $\alpha_p(\omega)$, this enhancement can reach $\sim 10^6$. Note that, within classical description, the dependence of SERS on nanoparticle size, coming from geometrical factor in α, is weak if the molecule is sufficiently close to nanoparticle surface.

The classical approach is valid for relatively large nanoparticles, where the effect of confining potential on electronic states is negligible. For nanoparticle sizes $\lesssim 10$ nm, the lifetime of SP is reduced due to discreteness of single-electron levels [17]. Landau damping of SP by single-particle excitations, accompanied by momentum transfer to the surface, results in a broadening of SP resonance peak by the amount of level spacing at the Fermi energy, $\gamma_s \sim v_F/R$ (v_F is the Fermi velocity), and in the corresponding reduction of the SP field amplitude. This effect can be treated semiclassically by incorporating the quantum-size correction γ_s in the Drude dielectric function of metal, $\epsilon(\omega) = 1 - \omega_p^2/\omega(\omega + i\gamma)$, where ω_p is bulk plasmon frequency. For even smaller *nanometer-sized* particles, the spatial distribution of local fields near the surface becomes important and semiclassical approach also fails. An adequate description of SERS in small nanoparticles requires microscopic approach. Such an approach is developed in this paper.

Our chief observation is that, in nanometer-sized noble-metal particles, SERS is determined by the *interplay between quantum-size and many-body effects*. The latter produces an opposite trend towards a *relative increase* of SERS in smaller particles. The underlying mechanism is related to a different effect of confining

potential on *d*-band and *sp*-band electron states in noble-metals. Namely, the deviation of potential well from the rectangular shape gives rise to a larger *effective* radius for the higher-energy *sp*-electrons [18]. As a result, in a *surface layer* of thickness $\Delta \sim 1$ Å, the *d*-electron population is diminished and, hence, the interband screening is strongly reduced [19]. This *underscreening* was observed, e.g., as faster, as compared to bulk metal, electron relaxation measured using ultrafast pump-probe spectroscopy [20]. The role of surface layer is further enhanced by the "spillover" effect of *sp*-band electron states that effectively increases the volume fraction of underscreened region while the localized *d*-electrons are mainly confined within bulk part of a nanoparticle.

To describe the spatial distribution of local fields near nanoparticle surface, we use the time-dependent local density approximation (TDLDA) [21] adopted for Ag nanoparticles in a dielectric medium. We find that the reduced screening in the surface layer leads to a substantial, relative to semiclassical result, increase of SERS from a molecule close to the surface. Remarkably, this many-body effect becomes more pronounced for smaller nanoparticle sizes.

2 Theory

Within microscopic approach, SERS should be formulated in terms of quantum transitions. In the absence of direct electron tunneling [16], the interactions within excited molecule-nanoparticle system are caused by *nonradiative transitions* with energy transfer between a molecule and a nanoparticle, similar to Forster transfer in two-molecule systems [22]. An electron-hole pair can nonradiatively recombine by transferring its energy to SP (and vice versa) via dynamically-screened Coulomb interaction [23]. Feynman diagrams of processes contributing to polarizability of molecule-nanoparticle system, $\tilde{\alpha}$, are shown in Fig. 1. These include: (a) incident photon with energy ω is absorbed and reemitted with energy ω_s by the molecule; (b) excited molecule nonradiatively recombines with energy transfer to SP in the nanoparticle, which emits a photon; (c) SP, excited by incident light, transfers its energy to the molecule, which emits a photon; and (d) after energy transfer from SP to molecule, the latter transfers the energy back to SP, which emits a photon. The system polarizability is (in operator form)

$$\tilde{\alpha} = \alpha + \alpha U \Pi + \Pi U \alpha + \Pi U \alpha U \Pi \qquad (1)$$

where α is the molecular polarizability, Π is density-density response function of a nanoparticle in medium, and U is the Coulomb potential. The Raman polarizability is obtained by calculating the matrix element of

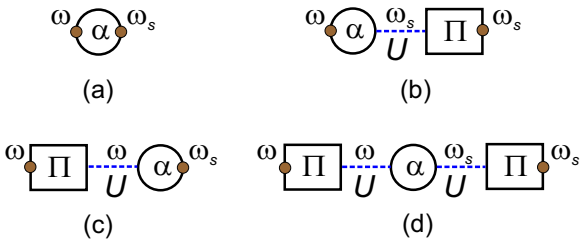

Figure 1: Nonradiative processes contributing to Raman scattering from a molecule-nanoparticle system.

$\tilde{\alpha}$ between incoming and outgoing photon states with energies ω and ω_s, respectively. The interaction of molecule with nanoparticle involves matrix elements $\langle e|\phi(\mathbf{r})|g\rangle$, where $|g\rangle$ and $|e\rangle$ stand for the molecule ground and excited electronic bands, respectively, and $\phi(\omega, \mathbf{r}) = \int d\mathbf{r}_1 d\mathbf{r}_2 U(\mathbf{r} - \mathbf{r}_1)\Pi(\omega, \mathbf{r}_1, \mathbf{r}_2)\phi_0(\mathbf{r}_2)$ is the nanoparticle response to external photon potential, $\phi_0(\mathbf{r})$. Since the length scale of $\phi(\mathbf{r})$ is much larger than the molecule size, we have $\langle e|\phi(\mathbf{r})|g\rangle \approx \boldsymbol{\mu}\nabla\phi(\mathbf{r}_0)$, where $\boldsymbol{\mu}$ is the dipole matrix element of corresponding molecular transition [24]. The averaging over random orientations of $\boldsymbol{\mu}$ can be accounted by assuming isotropic Raman polarizability tensor α. The nanoparticle contribution then factors out, $\tilde{\alpha} = \alpha M$, with

$$M = 1 + \frac{1}{E_0^2}\Big[\mathbf{E}_0 \cdot \nabla\phi(\omega, \mathbf{r}_0) + \mathbf{E}_0 \cdot \nabla\phi(\omega_s, \mathbf{r}_0) + \nabla\phi(\omega, \mathbf{r}_0) \cdot \nabla\phi(\omega_s, \mathbf{r}_0)\Big], \qquad (2)$$

where $\mathbf{E}_0$ is the electric field in the absence of nanoparticle. For incident field, $\mathbf{E}_i$, polarized along the z-axis, $\phi_0 = -eE_i r\cos\theta$, we have $\mathbf{E}_0 = \mathbf{E}_i/\epsilon_m$, where ϵ_m is the dielectric constant of medium. Note that for nanometer-sized particles, retardation effects can be ignored [17].

To evaluate the local potential $\phi(\omega, \mathbf{r})$ within TDLDA approach, we present it in the form

$$\phi(\omega, \mathbf{r}) = e^2 \int d^3r' \, \frac{\delta n(\omega, \mathbf{r}')}{|\mathbf{r} - \mathbf{r}'|}, \qquad (3)$$

where the induced density $\delta n(\mathbf{r}) = \int d\mathbf{r}'\Pi(\mathbf{r}, \mathbf{r}')\phi_0(\mathbf{r}') = \delta n_s(\mathbf{r}) + \delta n_d(\mathbf{r}) + \delta n_m(\mathbf{r})$ contains contributions from *sp*-electrons, *d*-electrons, and surrounding medium, respectively (hereafter we suppress frequency dependence).

We adopt the two-region model that combines a quantum-mechanical description for *sp*-band electrons and phenomenological treatment *d*-electrons with bulk-like ground-state density n_d in the region confined by $R_d < R$ [19]. This model has been used for calculations of polarizabilities of small Ag nanoparticles and clusters [25, 26], but it remains reliable for relatively large

electron numbers, $N > 1000$. The induced density of *sp*-band electrons is determined from

$$\delta n_s(\mathbf{r}) = \int d^3r' P_s(\mathbf{r},\mathbf{r}')\Big[\Phi(\mathbf{r}') + V_x'[n(r')]\delta n_s(\mathbf{r}')\Big], \quad (4)$$

where $\Phi = \phi_0 + \phi$ is the full potential, $P_s(\mathbf{r},\mathbf{r}')$ is the polarization operator for noninteracting *sp*-electrons, $V_x'[n(r')]$ is the (functional) derivative of the exchange-correlation potential and $n(r)$ is the ground-state electron density. The latter is obtained in a standard way by solving Kohn-Sham equations. To close the system, we need to express the full potential $\Phi(\mathbf{r})$ via $\delta n_s(\mathbf{r})$. This is accomplished be relating $\delta n_d(\mathbf{r})$ and $\delta n_m(\mathbf{r})$ back to $\Phi(\mathbf{r})$ as $e^2\delta n_d(\mathbf{r}) = \nabla\big[\chi_d(r)\nabla\Phi(\mathbf{r})\big]$ and $e^2\delta n_m(\mathbf{r}) = \nabla\big[\chi_m(r)\nabla\Phi(\mathbf{r})\big]$, where $\chi_d(r) = \frac{\epsilon_d - 1}{4\pi}\,\theta(R_d - r)$ is the interband susceptibility with the step function enforcing the boundary conditions and, correspondingly, $\chi_m(r) = \frac{\epsilon_m - 1}{4\pi}\,\theta(r - R)$ is the succeptibility of surrounding medium. The explicit relation can then be obtained by expanding Φ and δn in spherical harmonics and keeping only the dipole term. Leaving the details for a future publication [27], we can present Φ as

$$\Phi = \varphi_0 + \delta\varphi_0 + \delta\varphi_s, \quad (5)$$

where $\varphi_0 = \phi_0/\epsilon(r) = -eE_i r/\epsilon(r)$,

$$\delta\varphi_0(r) = \frac{1}{\epsilon(r)}\Big[-\beta(r/R_d)\phi_0(R_d)\,\lambda_d(1-2\lambda_m)/\eta + \beta(r/R)\phi_0(R)\,\lambda_m(1-a^3\lambda_d)/\eta\Big], \quad (6)$$

and

$$\delta\varphi_s(r) = \int dr' r'^2 K(r,r')\delta n_s(r'). \quad (7)$$

Here $\epsilon(r) = (\epsilon_d,\ 1,\ \epsilon_m)$ for r in the intervals $[(0,R),\ (R_d,R),\ (R,\infty)]$, respectively, and

$$\lambda_d = \frac{\epsilon_d - 1}{\epsilon_d + 2}, \quad \lambda_m = \frac{\epsilon_m - 1}{2\epsilon_m + 1}, \quad \eta = 1 - 2a^3\lambda_d\lambda_m, \quad (8)$$

with $a = R_d/R$. The kernel $K(r,r')$, relating the induced potential and density of *sp*-electrons, is given by

$$K(r,r') = \frac{e^2}{\epsilon(r)}\Big[u(r,r') - \beta(r/R_d)\Big[u(R_d,r') - 2a\lambda_m u(R,r')\Big]\lambda_d/\eta + \beta(r/R)\Big[u(R,r') - a^2\lambda_d u(R_d,r')\Big]\lambda_m/\eta\Big], \quad (9)$$

where $u(r,r') = \frac{4\pi r_<}{3r_>^2}$ is the dipole term of Coulomb potential expansion and $\beta(x) = x^{-2}\theta(x-1) - 2x\theta(1-x)$. The TDLDA equation (4) now takes the form

$$\delta n_s(r) = \int dr' r'^2 P_s(r,r')\Big[\varphi_0(r') + \delta\varphi_0(r')\Big] + \int dr' r'^2 P_s(r,r')\Big[\int dr'' r''^2 K(r',r'')\delta n_s(r'') + V_x'(r')\delta n_s(r')\Big]. \quad (10)$$

Note that $\delta\varphi_s(r)$ as well as the total potential $\Phi(r)$ are continuous at $r = R_d, R$.

Equations (5-10) determine self-consistently the spatial distribution of local potential near small noble-metal nanoparticles. Here $\delta\varphi_0(r)$ is the induced potential due to *d*-electrons and surrounding medium. Their effect on the *sp*-electron potential, $\delta\varphi_s(r)$, is encoded in the kernel $K(r,r')$. For $\epsilon_d = \epsilon_m = 1$, we have $K(r,r') = u(r,r')$ and $\delta\varphi_0(r) = 0$, recovering the case of simple metal particles in vacuum. If the molecule is not too close to the surface ($d \gtrsim 1$Å), i.e., there is no significant overlap between molecular orbitals and electronic states, then Eqs. (3) and (5-10) yield $\phi(r_0) = \frac{eE_i}{\epsilon_m r_0^2}\,\alpha_p$, where $\alpha_p = \frac{4\pi}{3eE_i}\int dr r^3\delta n(r)$ is the nanoparticle polarizability. In this case, Eq. (2) simplifies to

$$M = 1 + (1+\nu^2)[g(\omega) + g(\omega_s)] + (1+3\nu^2)g(\omega)g(\omega_s), \quad (11)$$

with $g = \alpha_p/r_0^3$ and $\nu = \cos\theta_0$. In this case, enhancement retains the same functional dependence on particle polarizability as in classical theory [6,7]; however, α_p is now determined microscopically.

3 Numerical results

In Figs. 2 and 3, we present our results for SERS enhancement factor for Ag nanoparticles in a medium with $\epsilon_m = 1.5$. Calculation were carried for number of electrons ranging from $N = 92$ to $N = 3028$, corresponding to particle diameters in the range $D \approx 1.4 - 4.5$ nm (to ensure spherical symmetry, only closed-shells "magic numbers" were used [28]). For such sizes, the Ag band-structure remains intact. The ground state energy spectrum and wave-functions were obtained by solving the Kohn-Sham equations for jellium model [21] with the Gunnarsson-Lundqvist exchange-correlation potential [29]; the interaction strength was appropriately modified to account for static *d*-band screening. These results were used as input in the numerical solution of TDLDA system (5-10). A more detailed description of numerical procedure will be reported elsewhere [27]. The ground state density $n(r)$ exhibited characteristic Friedel oscillations, while the spatial extent of spillover was $\simeq 3$ a.u. This value is somewhat smaller than for nanoparticles

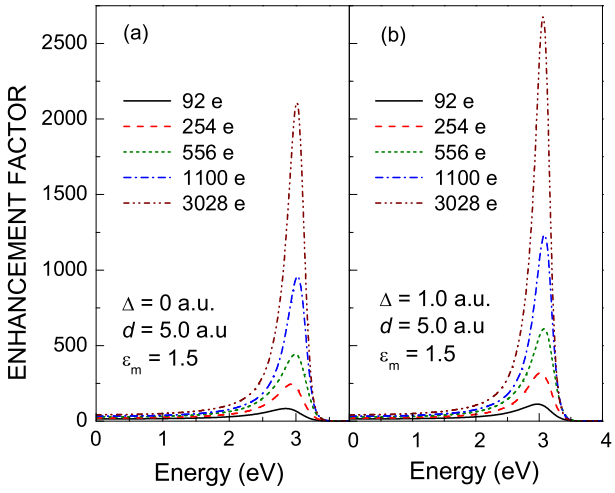

Figure 2: Enhancement factor for different nanoparticle sizes is shown with $\Delta = 0$ (a) and $\Delta = 1.0$ a.u. (b).

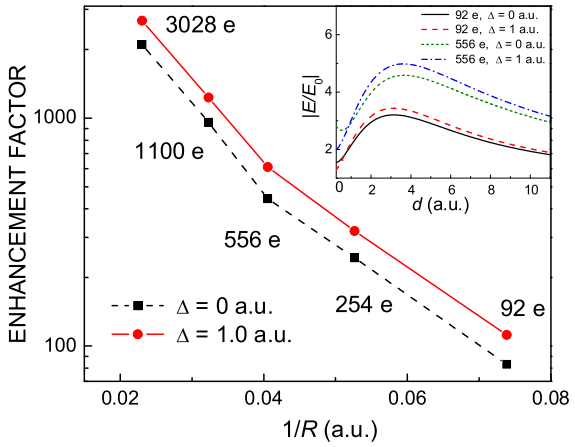

Figure 3: SERS at resonance frequency vs. nanoparticle size. Inset: Local field E vs. distance to surface.

in vacuum due to the additional screening of Coulomb interactions by surrounding medium. The molecule was located along z-axis ($\theta_0 = 0$) at a distance $d = 5$ a.u. from effective boundary with radius $R = r_s N^{1/3}$, where $r_s = (4\pi n/3)^{-1/3}$ ($r_s = 3.0$ a.u. for Ag), ensuring no direct overlap with the nanoparticle. In calculation of optical response, the experimental data for $\epsilon_d(\omega)$ in Ag was used [30], while surface layer thickness, $\Delta = R - R_d$, was varied, $\Delta = 0$ and 1.0 a.u., We also assumed that the Stokes shift is much smaller than $\gamma_s \sim v_F/R$ ($\gamma_s \simeq 0.5$ eV for $D = 3.0$ nm) and ignored the difference between ω and ω_s.

In Fig. 2, we plot the enhancement factor $|M|^2$ as a function of incident light energy for different nanoparticle sizes. To highlight the role of surface layer, the results for both $\Delta = 0$ and $\Delta = 1.0$ a.u. are shown in Fig. 2(a) and (b), respectively. Note that interband screening is reduced even for $\Delta = 0$ due to spillover of *sp*-band states into the potential barrier. The enhancement peak at SP resonance position, $\omega_{sp} \simeq 3.0$ eV, is well separated from the interband transitions onset for Ag at ≈ 4.0 eV. The general tendency is a decrease of SERS for smaller nanoparticles. This is mainly related to the Landau damping of SP which leads to a quite weak, $M^2 \sim 100$, enhancement for the smallest $D \approx 1.4$ nm nanoparticle. For larger particles, the damping decreases as $\sim v_F/R$, so the enhancement is stronger.

The effect of the surface layer on SERS is two-fold. The large contrast ratio of ϵ_d in the bulk and surface regions [$\epsilon_d(\omega_{sp}) \approx 5$] results in a lower *average* interband dielectric function, ϵ_d, which leads to a slight *blueshift* of peak position for $\Delta = 1.0$ a.u. ($\delta\omega_{sp} \sim 0.05$ eV). At the same time, the *magnitude* of enhancement *increases* significantly (in comparison to blueshift), although the resonance width stays unchanged. This is caused by the *underscreening* of SP field in the surface layer. The calculated local field, E, at resonance frequency is plotted in Fig. 3(inset) versus molecule-nanoparticle distance, $d = r_0 - R$. The gradual rise of field magnitude on the length scale of electron spillover replaces the discontinuity (for $\epsilon_d, \epsilon_m \neq 1$) of classical field at a sharp boundary. It can be seen that underscreening effect on SERS is strongest if a molecule is located at a close (several Å) distance from the nanoparticle. Note that even though the field enhancement itself is not big, its effect on Raman signal enhancement, $|M^2| \propto |E|^4$, is substantial.

The interplay between quantum-size (SP damping) and many-body (underscreening) contributions is most visible in the dependence of SERS on nanoparticle size, plotted in Fig. 3 at resonance frequency. While SERS amplitude drops by order of magnitude between $D \approx 4.5$ and 1.4 nm, this decrease is *slower* when surface layer effect is included. Indeed, the relative increase in SERS for $\Delta = 1.0$ a.u. is 25% for $N = 3028$, but 35% for $N = 92$. This is because the volume fraction of underscreened region is larger in smaller particles. Note, finally, that by keeping Δ constant for different nanoparticle sizes, we somewhat underestimated the many-body contribution to SERS. Indeed, for smaller nanoparticles, surface layer is thicker due to stronger deviations of the confining potential from rectangular shape.

As a concluding remark, we considered here a *non-resonant* Raman scattering, i.e., molecule energy in the intermediate state is much larger than ω_{sp}. In this case,

the biggest contribution to enhancement comes from the *back and forth* Coulomb energy transfer process between SP and molecule [see Fig. 1(d)]. For *resonant* coupling, the optical response of molecule-nanoparticle system is dominated by *multiple* transfer processes. This will be addressed in a future publication.

This work was supported by NSF under grants DMR-0305557 and NUE-0407108, by NIH under grant 5 SO6 GM008047-31, and by ARL under grant DAAD19-01-2-0014.

References

[1] For a recent review see G. S. Schatz and R. P. Van Duyne, in *Handbook of Vibrational Spectroscopy*, edited by J. M. Chalmers and P. R. Griffiths (Wiley, 2002) p. 1.

[2] S. Nie and S. R. Emory, Science **275**, 1102 (1997).

[3] K. Kneipp *et al.,* Phys. Rev. Lett. 78, 1667 (1997).

[4] Y . C. Cao, R. Jin, and C. A. Mirkin, Science **297**, 1536 (2002).

[5] M. Moskovits, Rev. Mod. Phys. **57**, 783 (1985).

[6] M. Kerker, D.-S. Wang, and H. Chew, Appl. Optics **19**, 4159 (1980).

[7] J. Gersten and A. Nitzan, J. Chem. Phys. **73**, 3023 (1980).

[8] K. Kneipp *et al.,* Chem. Rev. **99**, 2957 (1999), and references therein.

[9] A. M. Michaels, J. Jiang, and L. E. Brus, J. Phys. Chem. B **104**, 11965 (2000).

[10] M. Moskovits, L. Tay, J. Yang, T. Haslett, Top. Appl. Phys. **82**, 215 (2002).

[11] Z. Wang *et al.,* Proc. Nat. Acad. Sci. **100**, 8639 (2004).

[12] M. I. Stockman, L. N. Pandey, and T. F. George, Phys. Rev. B **53**, 2183 (1996).

[13] V. A. Markel *et al.,*, Phys. Rev. B **53**, 2425 (1996).

[14] H. Xu *et al.,* Phys. Rev. Lett. **83**, 4357 (1999).

[15] K. Li, M. I. Stockman, D. J. Bergman, Phys. Rev. Lett. **91**, 227402 (2003).

[16] Processes related to charge transfer (chemical mechanism) are out of scope of this paper, see A. Otto *et al.,* J. Phys. Cond. Matter **4**, 1143 (1992), and references therein.

[17] See, e.g., U. Kreibig and M. Vollmer, *Optical Properties of Metal Clusters* (Springer, 1995).

[18] B. N. J. Persson and E. Zaremba, Phys. Rev. B **31**, 1863 (1985).

[19] A. Liebsch, Phys. Rev. **48**, 11317 (1993).

[20] C. Voisin *et al.,* Phys. Rev. Lett. **85**, 2200 (2000).

[21] W. Ekardt, Phys. Rev. B **31**, 6360 (1985).

[22] J. R. Lakowicz, *Principles of Fluorescence Spectroscopy* (Plenum, 1999).

[23] T. V. Shahbazyan, I. E. Perakis, and J.-Y. Bigot, Phys. Rev. Lett. **81**, 3120 (1998).

[24] See, e.g., D. A. Long, *The Raman Effect* (Wiley, 2002).

[25] V. V. Kresin, Phys. Rev. **51**, 1844 (1995).

[26] J. Lerme *et al.,* Phys. Rev. Lett. **80**, 5105, (1998).

[27] V. N. Pustovit and T. V. Shahbazyan, to be published.

[28] E. Koch and O. Gunnarsson, Phys. Rev. B **54**, 5168, (1996)

[29] O. Gunnarsson and B. Lundqvist, Phys. Rev. B **13**, 4274 (1976).

[30] *Handbook of Optical Constants of Solids*, Ed. E. D. Palik (Academic Press, 1985).